HHS Public Access

Author manuscript

J Comput Chem. Author manuscript; available in PMC 2018 June 15.

Published in final edited form as:

J Comput Chem. 2017 June 15; 38(16): 1462–1471. doi:10.1002/jcc.24694.

Evaluation of the Hybrid Resolution PACE Model for the Study of Folding, Insertion and Pore Formation of Membrane Associated Peptides

Michael D. Ward[1], **Shivangi Nangia**[1], and **Eric R. May**[1]

[1]Department of Molecular and Cell Biology, University of Connecticut, Storrs, CT 06269

Abstract

The PACE force field presents an attractive model for conducting molecular dynamics simulations of membrane-protein systems. PACE is a hybrid model, in which lipids and solvents are coarse-grained consistent with the MARTINI mapping, while proteins are described by a united-atom model. However, given PACE is linked to MARTINI, which is widely used to study membranes, the behavior of proteins interacting with membranes has only been limitedly examined in PACE. In this study PACE is employed to examine the behavior of several peptides in membrane environments, namely WALP peptides, melittin and influenza hemagglutinin fusion peptide (HAfp). Overall, we find PACE provides an improvement over MARTINI for modeling helical peptides, based upon the membrane insertion energetics for WALP16 and more realistic melittin pore dynamics. Our studies on HAfp, which forms a helical hairpin structure, do not show the hairpin structure to be stable, which may point toward a deficiency in the model.

Graphical Abstract

The hybrid resolution PACE model has been applied to several well studied peptide-membrane systems. The simulations show that PACE provides a reasonably accurate model to study simple peptide topologies, such as single pass TM helices. However, we find PACE does not maintain the native helical hairpin structure of the influenza hemagglutinin fusion peptide, which may be caused by an unfavorable electrostatic interaction in the model.

Correspondence to: Eric R. May, eric.may@uconn.edu.

Additional Supporting Information may be found in the online version of this article.

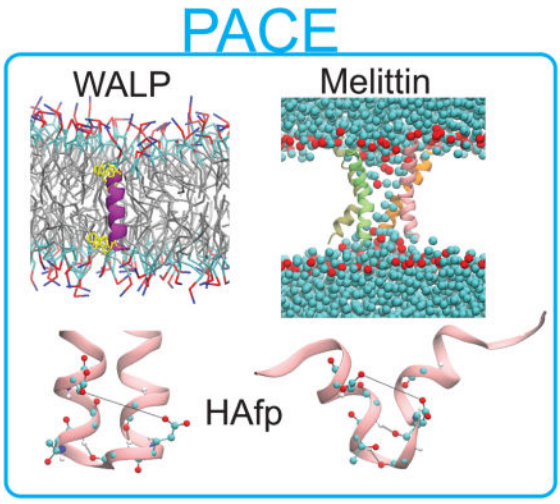

Keywords

Coarse grained models; hybrid resolution models; membranes; melittin; influenza hemagglutinin fusion peptide; WALP

Introduction

Molecular dynamics (MD) simulations of membrane protein systems can be informative of many biological processes, including ion transport,[1] cell signaling,[2] and protein translocation,[3] among others.[4] Recent studies have utilized MD to explore and validate complete models of enveloped virus particles including HIV-1[5] and Influenza A.[6]. While MD can be harnessed to perform rigorous kinetic,[7] thermodynamic[8] or mechanical[9] analyses on biological systems, the method can also be a great tool for understanding the qualitative features of a system at atomic resolution; a "computational microscope",[10] as it has been described.

However, a limitation of MD is the typical timescales of all-atom simulations are in the nanoseconds (ns) to microseconds (μs) range. These timescale limits are being pushed by advances in modern high performance architectures, GPU computing[11] and specialized hardware such as the ANTON/ANTON 2 machine.[12,13] All-atom simulations are often augmented by enhanced sampling methods to accelerate protein dynamics (recently reviewed in[14,15]) and improve convergence of computed properties. However, these methods may significantly increase the computational cost (e.g. replica-exchange, umbrella sampling), may obscure the gathering of kinetic/mechanistic information (e.g. replica-exchange) or may involve non-Boltzmann sampling that can complicate (or prevent) the calculation of thermodynamic quantities (e.g. metadynamics, accelerated MD, temperature-accelerated MD, adaptive-biasing force). While all-atom force-fields provide the most accurate classical description of biomolecules, coarse-grained (CG) models have been successfully developed to capture the essential physics, while omitting some atomic details that may not be critical to longer length scale phenomena. The utilization of CG models

provides a means to probe longer timescale and larger lengthscale biomolecular phenomena at a reduced computational cost. Of course the ability to access longer time scales is of little benefit if the models are not capable of providing a reasonable physical representation of the system.

Lipid systems has been an area where CG models have been particularly fruitful. Lipids are smaller than proteins and nucleic acids and do not fold into complex three-dimensional structures. The important features of lipids are their flexible hydrophobic tails attached to polar and charged head groups; properties which drive self-assembly into a variety of aggregated states, such as bilayers, micelles, and inverted hexagonal phases. These physical characteristics and ability to form aggregated states have been successfully modeled at descriptions less detailed than fully atomistic. The most detailed CG models are the united atom (UA) variety, in which only non-polar hydrogens are not explicitly represented. Popular UA models include those by Berger[16] and from the GROMOS force-field.[17] More aggressive CG models have been put forth by Klein,[18] Marrink (MARTINI)[19] and Voth[20] in which multiple heavy (non-hydrogen) atoms (−4) are mapped into a single CG interaction site. These models attempt to capture the net chemical properties of the atoms, which are represented by the CG beads. Whereas, even more aggressive CG models, referred to as mesoscopic models, focus on the bulk physical properties of the lipids. These models represent an individual lipid molecule by just a few CG particles, a notable model of this class is the three-bead model by Deserno.[21] In the mesoscopic models water is represented as a continuum solvent, which is also what is done in some CG models that use a lipid heavy atom 4-to-1 mapping.

Another approach to coarse-graining membranes is to completely remove the explicit representation of the bilayer and instead represent it implicitly as a continuum medium with a low dielectric constant. The implicit membrane representation is commonly predicated upon calculating the solvation free energy based upon a generalized Born formalism. The implicit membrane models may have a simple smoothing function[22] between the hydrophobic core and solvent dielectrics, or may have a more complex composition, with multiple slabs of different dielectric constants representing the different chemical environments of a bilayer, as function of bilayer depth.[23] An advantage of implicit membrane models is they are designed to be integrated with all-atom protein models. However, the lack of specific lipid-protein (and protein-solvent) interactions can be a downfall, as well as the inability to model heterogeneous membranes or membrane defects such as toroidal pores.

While these different CG models have their various strengths and weaknesses, the MARTINI model is one of the most widely used. The MARTINI model was initially developed for modeling lipids and surfactants,[24] and now offers hundreds of lipid types. The popularity of the model was established through studies which showed good agreement with experimental results in the study of lipid phase behavior[25,26] and membrane mechanical properties.[27] The force field has been extended to include proteins and DNA and has been utilized in the study of several membrane proteins including cytochrome proteins[28,29] and GPCRs.[30] However a limitation in the MARTINI protein model is that

secondary structure remains fixed through a simulation, so folding studies are not directly accessible.

Given that the MARTINI model provides a fast and reasonably accurate model for a wide range of lipids, it is desirable to couple this model with a higher resolution protein model that is suitable to study folding and secondary structure changes. Hybrid resolution models have recently been developed to achieve this goal, pairing MARTINI with the GROMOS all-atom force field[31,32] or the PACE UA force field.[33,34]

PACE was originally parameterized to be compatible with MARTINI water,[35] but was then extended to include MARTINI phosphatidylcholine (PC) lipids.[33] In the study that extended PACE to included PC lipids the tilting of WALP peptides in a transmembrane (TM) state was shown to be in reasonable agreement with experimental measurements. Dimerization of glycophorin A was also examined in a membrane environment and the simulated dimer structure was in excellent agreement with the NMR dimer structure. Further parameterization of the model to improve backbone solvation properties and the inclusion of partial charges on acidic and basic residues, allowed for successful folding of several peptides up to 73 residues long in an aqueous environment.[33,34] Subsequent studies of protein folding in aqueous environments include detailed analysis of the TRP-cage and WW-domain, which revealed the model is capable of capturing complex folding pathways involving both on- and off-pathway intermediates.[36] Also, β–amyloid fibril elongation was investigated with the PACE model using replica-exchange and kinetic network analysis, revealing mechanistic insights. [37]

The inclusion of PACE in the CHARMM-GUI[38,39] website has made the simulation of protein-membrane systems widely accessible. Currently, protein-bilayer systems can be constructed with 15 different lipid types with 4 different head groups (PC, PE, PS, PG).[39] Recent studies of membrane-protein systems using PACE include protonation-dependent conformational changes in lactose permease[40] and gating of the heat activated TRPV1 channel.[41]

While the availability and ease to setup membrane-protein systems through the CHARMM-GUI interface makes PACE an attractive model, there have been limited studies on the conformational dynamics of peptides in membrane environments with the latest version of PACE.[34] A recent study investigated the ability of PACE to capture the environmental sensitive folding behavior of the TMX3 peptide.[42] TMX3 is a 31 residue peptide which is largely disordered in water but becomes helical in membrane environments. In PACE, TMX3 showed similar degrees of folding in water and non-polar cyclohexane, which was explained by the inability of the CG MARTINI water to hydrogen bond with the protein backbone. They reasoned the lack of competition between backbone-backone and water-backbone hydrogen bonds leads to an overstabilization of folded structures in aqueous environments in PACE. In this work we will explore the folding characteristics of the helical WALP16, WALP19 and WALP23 peptides as well as the influenza hemagglutinin fusion peptide (HAfp), which forms a helical hairpin structure on micelles. In addition, we examine the dynamics of a tetramer of melittin peptides in a TM state for their ability to form transient water pores. We also performed simulations of the melittin and HAfp systems in

MARTINI to provide a basis for evaluation, while the WALP simulations are largely compared against previous all-atom simulations. The goal of this study is to evaluate the suitability of PACE for studying relatively small, but dynamic peptides in membrane environments.

Methods

The PACE force field has been described in detail previously,[33–35] we will only briefly summarize the main features of the model. PACE models solvents and lipids consistent with the MARTINI force field[19], while proteins are represented by a united atom model, where heavy atoms and polar hydrogens are explicitly represented. Cross-resolution terms are optimized against thermodynamic data, and partial charges are included on acidic and basic residues, which interact through Coulomb potentials in the UA representation, but CG and UA interactions are handled by an effective Lennard-Jones (LJ) potential. The Coulomb energies are calculated with a relative dielectric $\varepsilon_r = 15$, as is standard in MARTINI simulations with non-polarizable water.

A modified version of NAMD2.9[43] was used for all PACE simulations. Input files were generated through the CHARMM-GUI website,[38] which produces the standard six equilibration steps during which protein and lipid restraints are gradually released, as well as production run inputs. Parameters for the production runs include a 5-fs timestep with the neighbor list being updated every 10 steps. The electrostatic and van der Waals interactions were shifted to zero between 0 and 1.2 nm and 0.9 and 1.2 nm, respectively. The temperature was maintained at 303.15 K using a Langevin thermostat with a damping coefficient of 1/ps. Semi isotropic pressure coupling was applied using the Langevin piston method to maintain the pressure at 1 atm in the normal and lateral directions to the bilayer.

WALP Simulations

Five equilibrium simulations of 10 μs each were performed on WALP16, WALP19 and WALP23 peptides, which have sequences GWW$(LA)_5$WWA, GWW$(LA)_6$LWWA, and GWW$(LA)_8$LWWA, respectively. Each WALP peptide was simulated starting from an extended, TM configuration. Additionally, WALP16 and WALP19 were simulated from an extended structure starting ~2 nm above the membrane. The extended protein structures were generated using CHARMM.[44] The protein-membrane systems were generated with CHARMM-GUI to construct systems containing 250 total POPC lipids and enough water for a distance of at least 7 nm between the bilayer leaflets and their closest periodic image leaflet. Additionally, a 0.10 M NaCl concentration was used. TM structures were inserted into the membrane using the replacement method. Both termini were capped with acetyl (N-term) and N-methyl amide (C-term) groups. WALP16 and WALP19 were also simulated for 5 μs in a pure solvent system, starting from an extended conformation, to evaluate folding in the absence of a bilayer.

Steered Molecular Dynamics (SMD) was used to generate a series of snapshots along a de-insertion pathway, which would be subjected to umbrella sampling. This was done for WALP16, by pulling the center of mass of the peptide out of the membrane at a constant velocity of 1 Å/25 ns in the positive Z-direction. The SMD simulations applied a force

constant of 5 kcal/mol/Å^2 which was applied to the backbone atoms. The pull was done at a sufficiently slow rate to prevent any disruptions to the membrane that might not be able to re-equilibrate during umbrella sampling. Additionally, a Z-position restraint with a 0.5 kcal/mol/Å^2 force constant was applied to all phosphate groups of the lower leaflet of the membrane to prevent translation of the entire membrane in the positive Z-direction.

Umbrella sampling[45] was used to obtain a free energy profile describing the membrane insertion of WALP16. The distance between the center of mass (COM) of WALP16, based upon the α-carbons positions, and the center of mass of the bilayer, based upon all phosphate groups, was harmonically restrained in the Z-direction. 50 configurations were sampled, which spanned 0 to 50 Å COM separations, with approximately 1 Å spacing between windows. In each window the COM separation was maintained by a 5 kcal/mol/Å^2 force constant. Each window was simulated for 1 μs, and the reaction coordinate data was unbiased using the Weighted Histogram Analysis Method (WHAM)[46] software from Alan Grossfield (http://membrane.urmc.rochester.edu/content/wham) to obtain the potential of mean force (PMF).

Melittin Simulations

We simulated a tetramer of the antimicrobial peptide melittin in a tetrameric pore structure to evaluate whether PACE could accurately model the dynamics of a transient pore. The initial tetramer structure was obtained by backmapping[47] a system which was constructed in MARTINI (see below). The system consisted of 136 total DPPC lipids and a 0.10 M NaCl salt concentration. The PACE simulation was run for 5 μs.

We also ran a CG MARTINI[48,49] simulation with the GROMACS 4.6.5 package[50] of a system containing pre-arranged trans-membrane tetramer of melittin embedded in DPPC membrane. The system was generated using the insane.py script.[51] The melittin tetramer structure was generated by manipulating the crystal structure (PDB ID: 2MLT).[52] Specifically, four melittin peptide molecules were placed in a symmetric arrangement where all four peptides had their respective C-termini embedded in the upper bilayer leaflet. The tetramer was constructed by rotating and translating the melittin molecules such that the hydrophilic residues of each peptides faced each other while the hydrophobic residues faced outward toward the hydrophobic core of the DPPC bilayer, analogous to the protocol of Leveritt *at al.*[53] The bilayer contained 136 lipid molecules, and the system was solvated with 2928 CG MARTINI polarizable water particles and NaCl was added to a concentration of 0.1 M.

After the initial setup, the system was minimized using the steepest descent algorithm, followed by NVT equilibration simulation for 100 ns with position restraints on the peptides, while allowing the lipids, water and ions to relax. Next, all the restraints were removed and NPT simulations were performed for 5 μs using the Berendsen coupling scheme with the temperature maintained at 323 K and pressure kept at 1.0 bar with semi-isotropic coupling. The time constants for the pressure and temperature couplings were 3.0 and 1.0 ps, respectively, and the compressibility was set at 3×10^{-5} bar^{-1}. Electrostatic interactions were calculated using the Particle Mesh Ewald (PME) relative dielectric of $\varepsilon_r = 2.5$, in accordance with the protocols for MARTINI simulations using polarizable water. The

simulation was performed utilizing periodic boundary conditions in X,Y, and Z-directions, with a time step of 0.020 ps (except for NVT simulation where the time step was 0.010 ps). The nonbonded LJ interactions were smoothly shifted to zero between 0.9 and 1.3 nm.

HAfp Simulations

We studied the 23-residue variant of the HAfp N-terminal region, which has sequence GLFGAIAGFIEGGWTGMIDGWYG. The structure of the 23-residue HAfp has been determined by NMR in the presence of DPC micelles, and the structure displays a kinked topology, often referred to as a helical hairpin.[54] We evaluated the ability of PACE to properly fold HAfp in a membrane environment. We performed two 5 μs simulations starting from random extended conformations, one membrane bound and the other in solution ~2 nm above the membrane. The membrane was composed of 250 DLPC molecules in an attempt to match the chain length of lipids in a DPC micelle. Again, these systems were generated in CHARMM-GUI at a NaCl concentration of 0.1 M. Similar simulations were performed, but starting from the folded NMR structure (PDB ID: 2KXA). Six additional simulations starting from the folded, membrane bound state at different insertion depths were performed for 3–5μs each. The termini were charged in all simulations.

We also performed simulations of HAfp in the MARTINI force field using simulation parameters consistent with the MARTINI simulations of melittin. The system was generated from the HAfp NMR structure (PDB ID:2KXA), with charged termini. A bilayer of 250 DLPC lipids was constructed with the insane.py script and the system was solvated within polarizable water and ionized with NaCl at a 0.1 M concentration. Simulations were performed from starting configurations in which the peptide was placed ~2 nm above the membrane or in a membrane bound configuration. To construct the system topology a DSSP[55] structure file was supplied. The DSSP algorithm classified residues 2–21 as being helical, even though a kink occurs in the central region of the peptide. Simulations run using this native DSSP file caused the kinked helix to form a straight helix within the first ns of the simulations. Therefore, we created a modified DSSP file in which residues 10–12 were changed from type helix (H) to type loop (blank). Using this modified topology the system did not have a strong propensity for forming a straight helix and these are the simulations we analyzed for this study.

Trajectory Analysis

Trajectory analyses were performed using a combination of CHARMM, MDTraj[56] and GROMACS tools. Helicity measurements were taken every 1 ns using the COOR SECS function in CHARMM. Distance calculations between membrane and protein were done using MDTraj. Contacts between residues and the membrane were analyzed in CHARMM, using a cutoff of 5 Å. Tilt angles were calculated from the normalized dot product between the membrane normal and vector along the helical axis, described by the vector connecting the geometric center of the first four and last four residues. Representative snapshots were selected by using a script derived from the MDTraj example for finding a centroid. The algorithm computes all pairwise RMSDs between conformations and calculates a similarity score for each conformation. The similarity score exponentially decreases with increasing distance to favor conformations that are very close to a significant number of other

conformations. Melittin simulations in both PACE and MARTINI, were analyzed with the g_density tool from GROMACS, after re-aligning the membrane to the center for each snapshot of the trajectory. The density of water and at the center of the bilayer was computed using 11 slabs, and the sixth slab was treated as the center. The full density profiles used 100 slabs. HAfp kink angle calculations were performed with the QUICK function in CHARMM. The kink angle was computed between the three centers of mass defined by the Cα atoms in residues 3–6, 12–13 and 18–21. The choice to not use terminal residues was to avoid artifacts due to helix fraying.

Results and Discussion

WALP Peptides

WALP peptides are designed peptides,[57] which form a TM α-helix. Several all-atom simulations have been performed on WALP peptides interacting with membranes[58–61] and provide ample data to compare our PACE simulations against.

Folding & Insertion from Solution Phase—We performed equilibrium molecular dynamics simulations on three different length WALP peptides, WALP16, WALP19 and WALP23 to assess the ability of the PACE force field to properly fold the peptides into an α-helix structure and whether the environment (aqueous or membrane embedded) affected the folding. Furthermore, as these peptides are known to insert into membranes to form a TM configuration, we initiated simulations with an unfolded peptide in the solution phase to see if the peptides would spontaneously insert into the membrane phase and to see to what degree the folding and insertion process are coupled.

Simulations of WALP16 and WALP19 were initiated in an unfolded configuration in the solvent phase, approximately 2 nm away from the bilayer. The initial configuration for WALP16 is shown in Fig. 1a. Both WALP16 and WALP19 fold into a helical structure and spontaneously insert into the membrane (Fig. 1b–c). The peptides become buried under the phosphate head groups allowing the hydrophobic residues to partition from the polar solvent/headgroup region to the nonpolar lipid core. The WALP peptides remain inserted for the duration of the 10 μs simulations, but do not transition to a TM configuration.

PACE captures important aspects of the transition from solution to a membrane bound state. Previous studies done on WALP and other membrane inserting peptides have shown TRP-membrane interactions to be important for binding and insertion into the membrane.[62] Contact analysis shown in Fig. 1d and Fig. S1 reveals that TRP residues make the most contacts with the membrane leading up to insertion. This suggests that when the peptide associates with the membrane it is mainly caused by favorable TRP-membrane interactions. Most of the contacts are transient, until two TRP residues become anchored into the membrane. At this point the insertion of the peptide is very rapid (~1 ns), as evidenced by the steep drop in center of mass distance between peptide and phosphate head groups (Fig. S2).

An important aspect of evaluating PACE is whether the CG resolution of the solvent and membrane is sufficient to influence the protein structural properties. We do see that while

both WALP16 and WALP19 sample folded configurations in solvent, binding to the membrane shifts the populations toward more folded conformations for both WALP16 and WALP19 (Fig. 1e–f). This analysis was performed by comparing WALP16/19 in a pure solvent simulation against the membrane bound configuration. The structure of WALP peptides in aqueous solution is elusive to determine experimentally due to the hydrophobic aggregation properties. Atomistic simulations are suited to examine this problem, but differing results have been reported. Unbiased simulations have shown unfolding to occur in solution,[60] while metadynamics simulations have shown both folded and unfolded conformations are thermally accessible and the folded state is the free energy minimum.[63] There is a possibility that PACE is overstabilizing the helical content in the aqueous phase, but it does show that the membrane environment can influence the peptide structure.

Folding from TM State—In the above simulations initiated in the solvent we did not observe a transition to a TM helical conformation. This may be due to inadequate sampling (kinetic barriers) or due to the model favoring the interfacial configuration over a TM state (thermodynamic bias). To further evaluate this behavior, we initiated simulations with the peptides embedded in the membrane in an unfolded TM configuration (Fig. 2a). In addition to WALP16 and WALP19 we also simulated WALP23. The WALP16 peptide rapidly formed a TM helix (Fig. 2b), but it did not remain stable throughout the simulation. After approximately 4 μs WALP16 transitioned to an interfacial state, initially in a linear helical conformation, which then transitioned to a helical hairpin structure (Fig. 2c). The hairpin structure we observe is similar to hairpin structures observed in previous all-atom simulations of WALP peptides.[59,60]

Unlike WALP16, both WALP19 and WALP23 remain in a folded TM state through 10 μs simulations (Fig. 2d–e). An important structural feature of single pass TM helices is their orientation relative to the membrane normal. Different length helices tilt to different degrees to minimize hydrophobic mismatch. Tilt angles of WALP using PACE have been measured previously,[33] but not in a POPC bilayer, or since the recent force field optimization.[34] The tilt angle probabilities are shown in Fig. 2f, where it can be seen that WALP23 samples the highest tilt angles. For WALP19 and WALP23, the mean tilt angles are 12.1° and 14.6° respectively, which are in excellent agreement with the values of 12.5° and 14.9°, determined from all-atom enhanced sampling calculations in POPC membranes.[61]. However, we calculate WALP16 to have an average tilt angle of 13.2°, which does not agree with the aforementioned study that determined a 6.4° tilt angle for WALP16. Given that WALP16 undergoes a large transition from a TM helix to an interfacially bound state, we interpret the larger tilting to be due the peptide being frustrated in the TM state.

Free Energy of WALP16 Membrane Insertion—WALP16 is expected to remain stable in a TM configuration in POPC, and therefore we further investigated the energetics of WALP16 membrane insertion. We performed umbrella sampling calculations to determine the PMF to transport WALP16 from solvent to a TM configuration. Computing a converged PMF of partitioning a peptide from solvent to membrane is challenging in atomistic simulations, and can take an exorbitant amount computational resources.[64] Using PACE we are able to perform 1 μs sampling in each umbrella window, which may approximate up to

10 μs of sampling in an atomistic simulation, due to the inherent acceleration of protein dynamics in PACE.[34] We are able compute a converged PMF (Fig. 3a, S3), which shows there is a free energy minimum at both the TM state and also at the interfacial state, when the center of mass separation between the peptide and membrane is approximately 1.5 nm. The PMF is consistent with our unbiased simulations, which show WALP16 does not transition from the surface to a TM state, which can be attributed to both a barrier (~3 kcal/mol) and the TM state not having a lower free energy.

Atomistic simulations using the GROMOS force-field have been used to compute the PMF of WALP16 insertion into a POPC bilayer.[63] In that calculation, umbrella sampling was employed with 200 ns/window sampling along the insertion pathway. The PMF showed an overall insertion free energy change of approximately-35 kcal/mol, and the TM state was favored over the interfacial state by about 6 kcal/mol, though no significant barrier between the TM and interfacial state was observed. A subsequent study performed a multiscale sampling approach to compute the PMF of WALP16 insertion into a POPC bilayer.[65] A similar profile was computed using the multiscale sampling method the previous study, but there were some differences. The overall insertion free energy was reduced to about −30 kcal/mol and a small barrier (~2 kcal/mol) to transition from the interfacial to TM was observed. The ΔG between interfacial and TM states was about 6 kcal/mol, which was consistent in both PMFs.

In comparison to the AA PMFs of WALP16 insertion, it appears PACE is overstabilizing the interfacial state. This same problem was observed in pure MARTINI simulations, though there the interfacial state of WALP16 was globally stable and the barrier separating TM and interfacial states was considerably larger than what we compute for PACE.[63] In the same paper by Bereau *et al.,* they compute an atomistic insertion PMF, which shows a similar barrier between interfacial and TM configurations as we compute in PACE, but the TM state free energy is lower than the interfacial state by ~7 kcal/mol. The CG-PLUM model is also presented by Bereau *et al.,* which shows a downhill PMF of insertion, similar to the atomistic PMF, though that model does not produce a barrier between interfacial and TM states, and it produces a smaller ΔG of insertion by about 13 kcal/mol (ΔG = −22 PLUM; ΔG = −35 GROMOS), similar to PACE.

While PACE shows a significant improvement over MARTINI, the inability to predict the TM state as globally stable is troubling. A potential source of error in the PACE calculation may be due to the MARTINI representation of POPC lipids. We have used the historical five-bead representation of the oleoyl tail, though a four bead model has been recently introduced.[51] In the study by Bereau *et al.,* they compared the five-bead and four-bead models, and found that switching to the four-bead POPC model stabilized the TM state of WALP16 by nearly 10 kcal/mol. It is likely the inability of POPC to thin sufficiently to match the hydrophobic thickness of WALP16 in an ideal α-helical conformation is resulting in raising the energy of the TM state. From our umbrella sampling data, we examined the helicity and peptide end-to-end distance in the two minima and find that at the TM state the peptide is extended and does not sample conformations with as high helical content as at the interface (Fig. 3b.). With the thinner four-bead model WALP16 would likely not have to extend and break its helix to span the membrane. Thus, if we observed a similar degree of

stabilization by switching to the four-bead model, we would expect our PACE PMF to be in excellent agreement with the atomistic PMF from Bereau *et al.*

Melittin

Antimicrobial peptides (AMP) are of great interest for their potential antibiotic properties, and hence understanding their mechanism of action is of great importance. Melittin is a well studied AMP, which has been shown to form pores within membranes that are transient at low peptide:lipid ratios, but can be stabilized at higher peptide concentrations.[66,67] A transient melittin pore has been observed in long-time scale atomistic MD simulations, starting from a tetrameric TM orientation.[53] Simulations using MARTINI have also shown formation of transient melittin pores, though high peptide:lipid (1:21) ratios were required and only a single peptide was observed in a TM configuration.[68] We have utilized PACE to simulate a tetramer of melittin in a TM state embedded in a DPPC bilayer, to evaluate if water could permeate into the membrane interior and to what extent the protein dynamics were qualitatively similar to multi-μs all-atom simulations. We also performed simulations using MARTINI from the same starting tetramer configuration to evaluate what benefits PACE may have over a pure MARTINI representation.

In comparing our PACE and MARTINI simulations, we find that in PACE the peptides can adopt more varied orientations, whereas the peptides in MARTINI remain quite stable in the TM state. Furthermore, the PACE simulations show the ability to form transient water solvated pores, while the MARTINI simulation displays only minimal amounts of water permeation into the middle of the membrane. The water and phosphate densities for both PACE and MARTINI are shown in Fig. 4a–b, respectively, where the densities are calculated for each μs of the simulations. To further understand the pore dynamics we calculated the density at the center of the membrane every ns (Fig. 4c). Snapshots from the PACE simulations are shown which depict a configuration when a peptide has moved into a more lateral orientation (Fig. 4d), when the pore is well solvated and lipid phosphate groups have moved toward the bilayer center (Fig. 4e), and when the pore center is desolvated (Fig. 4f). Overall the PACE peptide and pore dynamics are qualitatively similar to those observed in all-atom simulations,[69] whereas the melittin peptides in the MARTINI simulations appear to be overly stable. It may be possible to optimize the MARTINI model by removing or reducing secondary structure restraints to increase peptide flexibility, but the lack of water permeation may indicate the peptide interactions are too attractive, which would require a more extensive re-parameterization. The PACE model shows promising characteristics in modeling oligomeric TM helical pore structures and warrants further investigation.

HAfp

While PACE performs well in modeling the simple α-helical WALP peptides and the slightly kinked melittin, we wanted to explore the applicability of PACE to a more complex protein structure in a membrane bound state. The influenza hemagglutinin fusion peptide (HAfp) provides a more complex protein structure to analyze. Based upon an NMR structure, the 23-residue HAfp peptide adopts a helical hairpin (kinked) conformation, when bound to a micelle.[54] We have conducted simulations of the 23-residue HAfp in solution and in the presence of a DLPC bilayer to determine the ability of PACE to fold into and

maintain a sharply kinked conformation consistent with the NMR structure. Our simulations entailed starting from folded and unfolded states, in solution and embedded into the bilayer, as well as starting from the folded configuration embedded in the bilayer at a range of insertion depths between 8 to 20 Å from the bilayer midplane. The HAfp peptide did not maintain a structure highly similar to the NMR structure in any of our simulations. Overall our findings show that HAfp prefers a straight helical conformation on the membrane (Fig. 5a–b), and while it samples a wide range of kink angles in solution (Fig. 5b) the angle of kinking is not as severe as the NMR hairpin structure, which is around 40°. The simulation that started with HAfp folded on the membrane does maintain a kinked conformation during the first μs, during which it samples a much narrower range of kink angles than during the solution simulation. However, even during the first μs of the membrane bound simulation the kink angle is around 60°, which is considerably larger than the NMR structure kink angle.

It should be noted that the configuration of HAfp is rather complex, as variety of factors including peptide sequence, peptide length, pH, and detergent/lipid composition can effect the peptide structure.[70] For the 23-residue HAfp, subpopulations of more open configurations have been detected by NMR. On a micelle at pH 4 an open structure was shown to be in equilibrium with the hairpin structure, with the open state constituting ~20% of the population.[71] Whereas on a bilayer at neutral pH the hairpin and a semi-closed conformations were shown to be in equilibrium, with the semi-closed state constituting ~30% of the population.[72] The kink angle in the semi-closed conformation is ~20° wider than the hairpin kink angle, which may correlate with our observation of structures having kink angles around 60°. Nonetheless the tight hairpin structure is the dominant species in these studies and inability of PACE to show the hairpin as a stable structure is in disagreement with experiments.

It has been acknowledged that PACE may overstabilize protein hydrogen bonds[37,42] due to the inability for the water or lipids to form hydrogen bonds with the protein. This results in random coil configurations being disfavored and may also be driving HAfp toward a straight helix. Another concern is that even when HAfp is forming a kinked structure it is not consistent with the dominant NMR observed structure. To try to understand why the hairpin is so rapidly destabilized in the PACE simulations we closely examined the initial 10 ns of the membrane bound simulation. When comparing the NMR structure (Fig. 5c) to the structure at 10 ns (Fig. 5d), there is a switch in the hydrogen bonds in the kinking region (residue 11–13). In the NMR structure GLY12 forms *i*-*i*+4 H-bonds with both GLY8 and GLY16, whereas in the 10 ns structure the bonding has switched to GLU11-GLY16 and GLY12-THR15, causing a change to a more open kink angle. A contributing factor to this switch may be the interaction between the only two charged residues, GLU11 and ASP19. The change in distance between ASP19 and GLU11 is highly correlated with the changes in the hydrogen bonding distances around the kink, as is shown in Fig. 5e. In the NMR structure the minimal distance between any of the GLU/ASP carboxylic acid oxygens is 8.85 Å, which is at a maximum in the PMF of ASP/GLU sidechain separation distance in the latest PACE parameterization, which includes partial charges.[34] In the 10 ns structure the distance has decreased to 6.8 Å, which is actually a minimum in the PACE ASP-GLU sidechain separation PMF. This is a somewhat non-intuitive finding given that the expectation for bringing two negatively charged side chains into closer proximity would be a

destabilizing effect, or at the least a flat interaction until they are close enough to repulse, which is what the all-atom OPLS PMF shows. The maximum appearing in the PACE PMF which does not appear in the OPLS PMF, may be inconsequential to many systems, but it may be having an undesired effect on the HAfp structure and causing it to deviate from the native hairpin configuration.

While PACE does not maintain a tight hairpin structure for HAfp we investigated whether MARTINI could be suitable for modeling the HAfp-membrane system. We ran analogous simulations to the PACE simulations where the kinked HAfp was started on a membrane and also ~2 nm above a DLPC membrane. The simulations started in solution rapidly associate (within 20 ns) with the membrane, while the simulations started on the membrane remain in a membrane-associated state throughout the simulation. The HAfp kink angle probability distribution for MARTINI is compared with the PACE simulations in Fig. S4. The MARTINI simulation does not maintain a tight helical hairpin, but produces a broad angular distribution with a maximum around 100°. The peaks in the MARTINI angle distribution coincide with peaks in the PACE simulations and therefore similar substates may be sampled by the different force fields. The broadness in the MARTINI distribution indicates rapid sampling of a wide range of conformations, which does not appear to be well supported by the majority of studies on the 23-residues HAfp by NMR[54,71] or atomistic MD.[73,74]

Conclusions

In this work we have examined the ability of PACE to model membrane peptide interactions for several well studied peptides. Our investigation of the designed WALP peptides show that an interfacially bound configuration is overstabilized in PACE, though we believe the stability of this state would be diminished by switching to the four-bead POPC MARTINI model. The tilt angles of WALP19 and WALP23 are in excellent agreement with all-atom simulations. Our studies of the antimicrobial melittin peptide have shown that a TM tetrameric pore modeled in PACE shows behaviors qualitatively consistent with all-atom simulations and offers significantly improved protein dynamics compared with MARTINI. Our studies on the influenza hemagglutinin fusion peptide showed PACE did not favor the helical hairpin structure determined by NMR. A possible source of inaccuracy is the introduction of partial charges on only the charged residues. For negatively charged side chains there is a maximum in the separation distance PMF, which may drive conformational changes away from native structures. Overall PACE is a promising model for studying membrane-peptide dynamics, though further refinement of the charged interactions and compensating for the inability of CG particles to hydrogen-bond with the protein are avenues which could potentially improve the accuracy of this force field.

Supplementary Material

Refer to Web version on PubMed Central for supplementary material.

Acknowledgments

The work has been supported by the National Institutes of Health through grants K22AI099163 and R35GM119762. Computational resources have been provided through the University of Connecticut Booth Engineering Center for Advanced Technology.

References and Notes

1. Ostmeyer J, Chakrapani S, Pan AC, Perozo E, Roux B. Nature. 2013; 501:121–124. [PubMed: 23892782]
2. Dror RO, Arlow DH, Maragakis P, Mildorf TJ, Pan AC, Xu H, Borhani DW, Shaw DE. Proc Natl Acad Sci USA. 2011; 108:18684–18689. [PubMed: 22031696]
3. Gumbart J, Chipot C, Schulten K. Proc Natl Acad Sci USA. 2011; 108:3596–3601. [PubMed: 21317362]
4. Chavent M, Duncan AL, Sansom MS. Curr Opin Struct Biol. 2016; 40:8–16. [PubMed: 27341016]
5. Zhao G, Perilla JR, Yufenyuy EL, Meng X, Chen B, Ning J, Ahn J, Gronenborn AM, Schulten K, Aiken C, et al. Nature. 2014; 497:643–646.
6. Reddy T, Shorthouse D, Parton DL, Jefferys E, Fowler PW, Chavent M, Baaden M, Sansom MSP. Structure. 2015; 23:584–597. [PubMed: 25703376]
7. Weber JK, Jack RL, Pande VS. J Am Chem Soc. 2013; 135:5501–5504. [PubMed: 23540906]
8. May ER, Arora K, Brooks CL III. J Am Chem Soc. 2014; 136:3097–3107. [PubMed: 24495192]
9. May ER, Brooks CL III. Phys Rev Lett. 2011; 106:188101. [PubMed: 21635128]
10. Lee EH, Hsin J, Sotomayor M, Comellas G, Schulten K. Structure. 2009; 17:1295–1306. [PubMed: 19836330]
11. Friedrichs MS, Eastman P, Vaidyanathan V, Houston M, Legrand S, Beberg AL, Ensign DL, Bruns CM, Pande VS. J Comput Chem. 2009; 30:864–872. [PubMed: 19191337]
12. Shaw, DE., Grossman, JP., Bank, JA., Batson, B., Butts, JA., Chao, JC., Deneroff, MM., Dror, RO., Even, A., Fenton, CH., et al. Proceedings of the International Conference for High Performance Computing, Networking, Storage and Analysis. Ieee; 2014. p. 41-53.
13. Shaw DE, Chao JC, Eastwood MP, Gagliardo J, Grossman JP, Ho CR, Lerardi DJ, Kolossváry I, Klepeis JL, Layman T, et al. Commun ACM. 2008; 51:91–7.
14. Mori T, Miyashita N, Im W, Feig M, Sugita Y. BBA - Biomembranes. 2016:1–54.
15. Abrams C, Bussi G. Entropy. 2014; 16:163–199.
16. Berger O, Edholm O, Jähnig F. Biophys J. 1997; 72:2002–2013. [PubMed: 9129804]
17. Chiu SW, Pandit SA, Scott HL, Jakobsson E. J Phys Chem B. 2009; 113:2748–2763. [PubMed: 19708111]
18. Shelley JC, Shelley MY, Reeder RC, Bandyopadhyay S, Moore PB, Klein ML. J Phys Chem B. 2001; 105:9785–9792.
19. Marrink SJ, Risselada HJ, Yefimov S, Tieleman DP, de Vries AH. J Phys Chem B. 2007; 111:7812–7824. [PubMed: 17569554]
20. Izvekov S, Voth GA. J Phys Chem B. 2005; 109:2469–2473. [PubMed: 16851243]
21. Cooke IR, Kremer K, Deserno M. Phys Rev E Stat Nonlin Soft Matter Phys. 2005; 72:011506–4. [PubMed: 16089969]
22. Im W, Feig M, Brooks CL III. Biophys J. 2003; 85:2900–2918. [PubMed: 14581194]
23. Tanizaki S, Feig M. J Chem Phys. 2005; 122:124706. [PubMed: 15836408]
24. Marrink SJ, de Vries AH, Mark AE. J Phys Chem B. 2004; 108:750–760.
25. Marrink SJ, Risselada J, Mark AE. Chem Phys Lipids. 2005; 135:223–244. [PubMed: 15921980]
26. May ER, Kopelevich DI, Narang A. Biophys J. 2008; 94:878–890. [PubMed: 17921207]
27. May E, Narang A, Kopelevich D. Phys Rev E. 2007; 76:021913.
28. Arnarez C, Mazat JP, Elezgaray J, Marrink SJ, Periole X. J Am Chem Soc. 2013; 135:3112–3120. [PubMed: 23363024]
29. Arnarez C, Marrink SJ, Periole X. Scientific Reports. 2013; 3:1263. [PubMed: 23405277]

30. Johnston JM, Wang H, Provasi D, Filizola M. PLoS Comput Biol. 2012; 8:e1002649. [PubMed: 22916005]
31. Rzepiela AJ, Louhivuori M, Peter C, Marrink SJ. Phys Chem Chem Phys. 2011; 13:10437–12. [PubMed: 21494747]
32. Wassenaar TA, Ingólfsson HI, Prieβ M, Marrink SJ, Schäfer LV. J Phys Chem B. 2013; 117:3516–3530. [PubMed: 23406326]
33. Wan CK, Han W, Wu YD. J Chem Theory Comput. 2012; 8:300–313. [PubMed: 26592891]
34. Han W, Schulten K. J Chem Theory Comput. 2012; 8:4413–4424. [PubMed: 23204949]
35. Han W, Wan CK, Jiang F, Wu YD. J Chem Theory Comput. 2010; 6:3373–3389. [PubMed: 26617092]
36. Han W, Schulten K. J Phys Chem B. 2013; 117:13367–13377. [PubMed: 23915394]
37. Han W, Schulten K. J Am Chem Soc. 2014; 136:12450–12460. [PubMed: 25134066]
38. Lee J, Cheng X, Swails JM, Yeom MS, Eastman PK, Lemkul JA, Wei S, Buckner J, Jeong JC, Qi Y, et al. J Chem Theory Comput. 2015; 12:405–413. [PubMed: 26631602]
39. Qi Y, Cheng X, Han W, Jo S, Schulten K, Im W. J Chem Inf Model. 2014; 54:1003–1009. [PubMed: 24624945]
40. Jewel Y, Dutta P, Liu J. Proteins. 2016:1–8.
41. Zheng W, Qin F. J Gen Physiol. 2015; 145:443–456. [PubMed: 25918362]
42. Jia Z, Chen J. J Comput Chem. 2016; 37:1725–1733. [PubMed: 27130454]
43. Phillips JC, Braun R, Wang W, Gumbart J, Tajkhorshid E, Villa E, Chipot C, Skeel RD, Kalé L, Schulten K. J Comput Chem. 2005; 26:1781–1802. [PubMed: 16222654]
44. Brooks BR, Brooks CL III, Mackerell AD Jr, Nilsson L, Petrella RJ, Roux B, Won Y, Archontis G, Bartels C, Boresch S, et al. J Comput Chem. 2009; 30:1545–1614. [PubMed: 19444816]
45. Torrie GM, Valleau JP. J Comput Phys. 1977; 23:187–199.
46. Roux B. Comp Phys Comm. 1995; 91:275–282.
47. Wassenaar TA, Pluhackova K, Böckmann RA, Marrink SJ, Tieleman DP. J Chem Theory Comput. 2014; 10:676–690. [PubMed: 26580045]
48. Monticelli L, Kandasamy SK, Periole X, Larson RG, Tieleman DP, Marrink SJ. J Chem Theory Comput. 2008; 4:819–834. [PubMed: 26621095]
49. de Jong DH, Singh G, Bennett WFD, Arnarez C, Wassenaar TA, Schäfer LV, Periole X, Tieleman DP, Marrink SJ. J Chem Theory Comput. 2013; 9:687–697. [PubMed: 26589065]
50. Hess B, Kutzner C, Van Der Spoel D, Lindahl E. J Chem Theory Comput. 2008; 4:435–447. [PubMed: 26620784]
51. Wassenaar TA, Ingólfsson HI, Böckmann RA, Tieleman DP, Marrink SJ. J Chem Theory Comput. 2015; 11:2144–2155. [PubMed: 26574417]
52. Terwilliger TC, Eisenberg D. J Biol Chem. 1982; 257:6010–6015. [PubMed: 7076661]
53. Leveritt JM, Pino-Angeles A, Lazaridis T. Biophys J. 2015; 108:2424–2426. [PubMed: 25992720]
54. Lorieau JL, Louis JM, Bax A. Proc Natl Acad Sci USA. 2010; 107:11341–11346. [PubMed: 20534508]
55. Kabsch W, Sander C. Biopolymers. 1983; 22:2577–2637. [PubMed: 6667333]
56. McGibbon RT, Beauchamp KA, Harrigan MP, Klein C, Swails JM, Hernández CX, Schwantes CR, Wang LP, Lane TJ, Pande VS. Biophys J. 2015; 109:1528–1532. [PubMed: 26488642]
57. Killian JA. FEBS Letters. 2003; 555:134–138. [PubMed: 14630333]
58. García AE, Onuchic JN. Proc Natl Acad Sci USA. 2003; 100:13898–13903. [PubMed: 14623983]
59. Im W, Brooks CL III. Proc Natl Acad Sci USA. 2005; 102:6771–6776. [PubMed: 15860587]
60. Ulmschneider MB, Doux JPF, Killian JA, Smith JC, Ulmschneider JP. J Am Chem Soc. 2010; 132:3452–3460. [PubMed: 20163187]
61. Kim T, Im W. Biophys J. 2010; 99:175–183. [PubMed: 20655845]
62. Nymeyer H, Woolf TB, García AE. Proteins. 2005; 59:783–790. [PubMed: 15828005]
63. Bereau T, Bennett WFD, Pfaendtner J, Deserno M, Karttunen M. J Chem Phys. 2015; 143:243127–12. [PubMed: 26723612]

64. Neale C, Hsu JCY, Yip CM, Pomès R. Biophys J. 2014; 106:L29–31. [PubMed: 24739184]
65. Bereau T, Kremer K. J Phys Chem B. 2016; 120:6391–6400. [PubMed: 27138459]
66. Lee MT, Hung WC, Chen FY, Huang HW. P Natl Acad Sci Usa. 2008; 105:5087–5092.
67. Lee MT, Sun TL, Hung WC, Huang HW. Proc Natl Acad Sci USA. 2013; 110:14243–14248. [PubMed: 23940362]
68. Santo KP, Irudayam SJ, Berkowitz ML. J Phys Chem B. 2013; 117:5031–5042. [PubMed: 23534858]
69. Leveritt JM III, Pino-Angeles A, Lazaridis T. Biophys J. 2015; 108:2424–2426. [PubMed: 25992720]
70. Worch R. Acta Biochimica Polonica. 2014; 61:421–426. [PubMed: 25195144]
71. Lorieau JL, Louis JM. Proc Natl Acad Sci USA. 2012; 109:19994–19999. [PubMed: 23169643]
72. Ghosh U, Xie L, Jia L, Liang S, Weliky DP. J Am Chem Soc. 2015; 137:7548–7551. [PubMed: 26039158]
73. Brice AR, Lazaridis T. J Phys Chem B. 2014; 118:4461–4470. [PubMed: 24712538]
74. Baylon JL, Tajkhorshid E. J Phys Chem B. 2015; 119:7882–7893. [PubMed: 25996559]

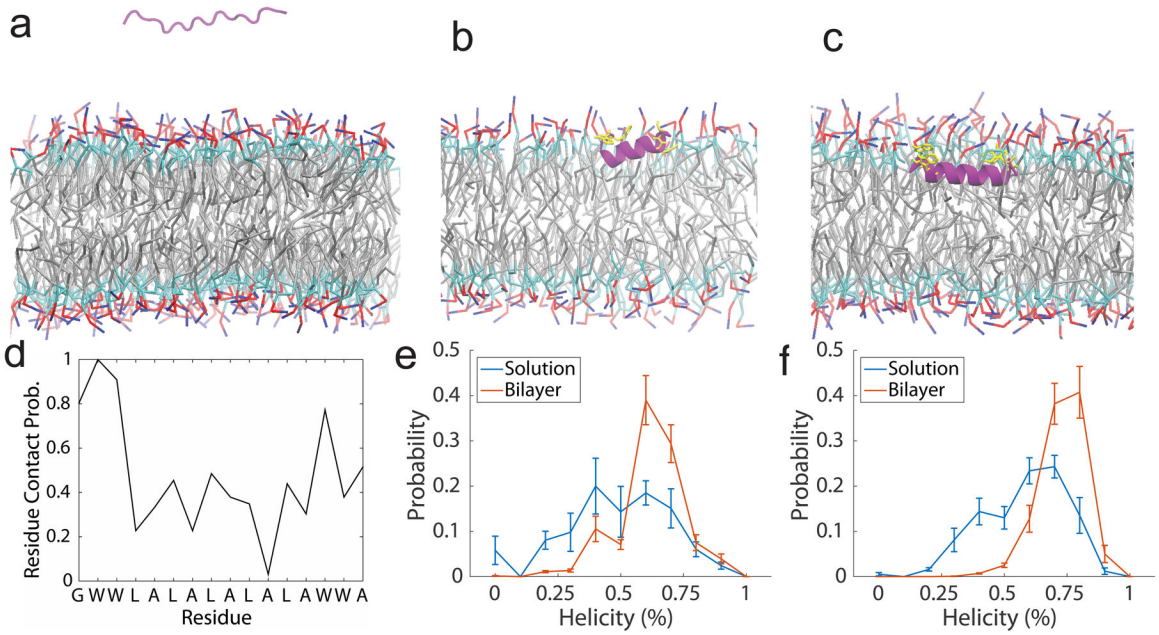

Figure 1.

Folding of WALP16 and WALP19 from solution. a) Initial structure for the WALP16 folding simulation. b) WALP16 and WALP19 (c) membrane bound centroid structures. d) Normalized contact probability for WALP16 during the initial membrane binding (first 1.3 μs) phase of simulation. e–f) Helical probabilities for WALP16 (e) and WALP19 (f) for when the peptide in solution and membrane bound. Helical probabilities were computed over 5 μs of data. The simulations were divided into 1 μs blocks from which the mean probabilities and standard errors (represented by the errorbars), were computed. TRP residues are shown in yellow in (b) and (c). Membrane coloring: tails=silver, glycerol=cyan, phosphate=red, choline=blue.

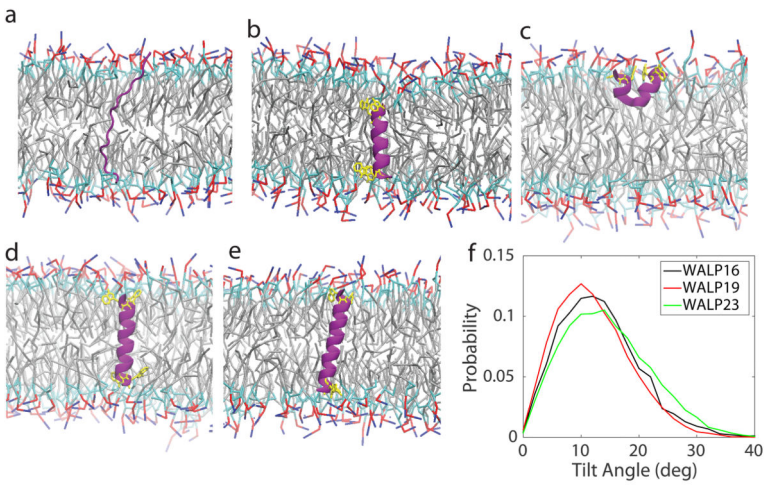

Figure 2.

WALP folding from a TM state. a) Initial configuration for WALP16 TM folding simulation. WALP16 initially folds to a TM helix (b), but transitions to a surface bound helical hairpin (c) after ~4 μs. WALP19 (d) and WALP23 (e) remain in a TM helical state for the full 10 μs simulations. f) Tilt angle distributions for WALP peptides. Distributions were calculated between 500 ns and 10 μs for WALP19 and WALP23 and between 500 ns and 4 μs for WALP16.

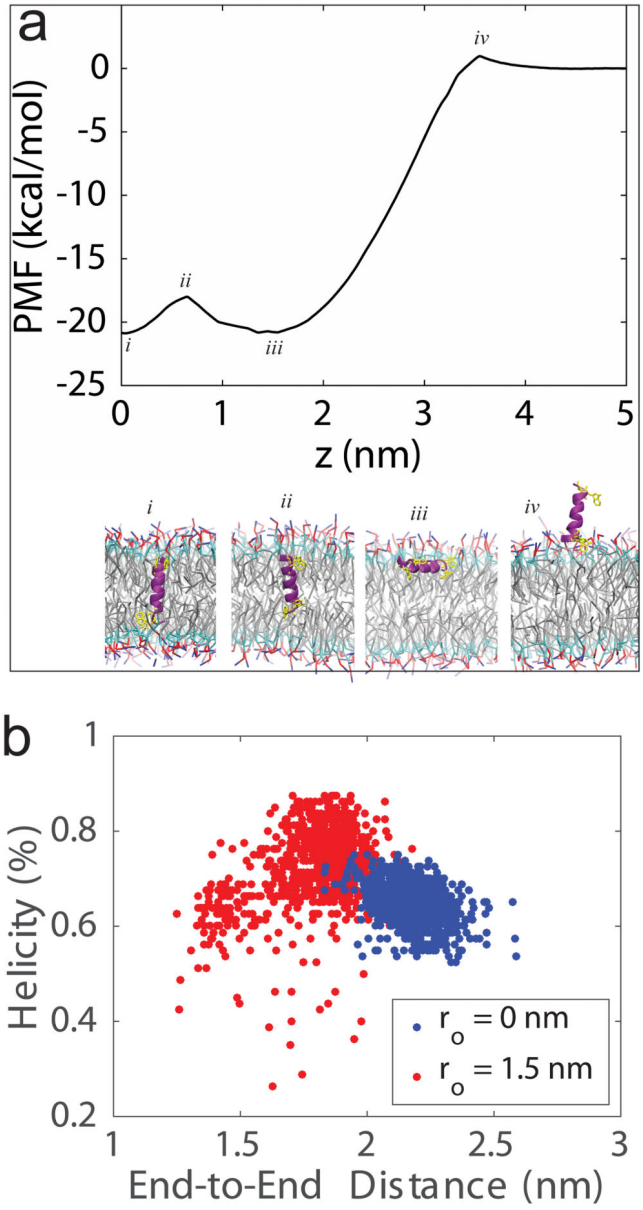

Figure 3.

WALP16 insertion energetics. a) The PMF of WALP16 membrane insertion shows equal free energy minima at the TM and interface states. Centroid structures from the umbrella sampling windows corresponding to minima and maxima are indicated by roman numerals and shown below. b) The peptide end-to-end distance and helicity for the umbrella sampling window when the center of mass separation was restrained to 0 nm (TM) and 1.5 nm (interfacial). Data was analyzed between 200–1000 ns, the helicity values are smoothed over 5 ns, to remove the discreteness of the helicity values.

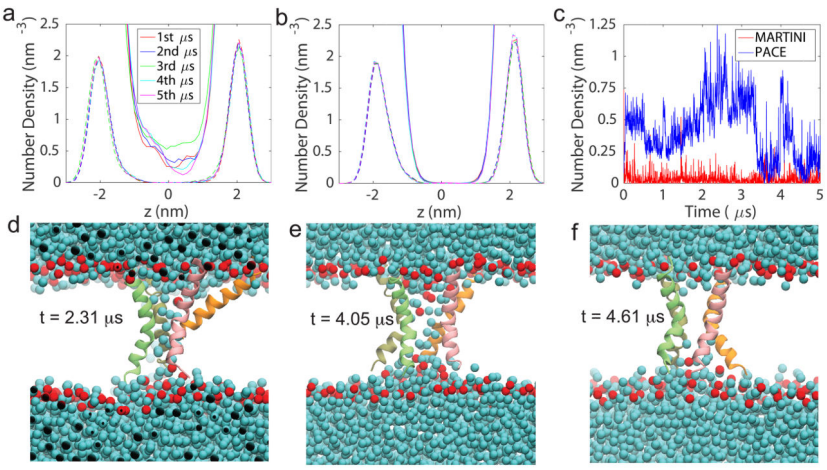

Figure 4.

TM melittin tetramer in PACE and MARTINI. Water (solid lines) and phosphate (dashed lines) number density in PACE (a) and MARTINI (b) for each μs of the simulations. The water density is multiplied by four to account of the CG water mapping. Densities were computed using 100 slabs. c) Density of water at the center of the bilayer using 11 slabs, again multiplied by 4. d–f) Snapshots from the PACE simulation at various time points, CG waters are represented as cyan spheres and lipid phosphate groups as red spheres.

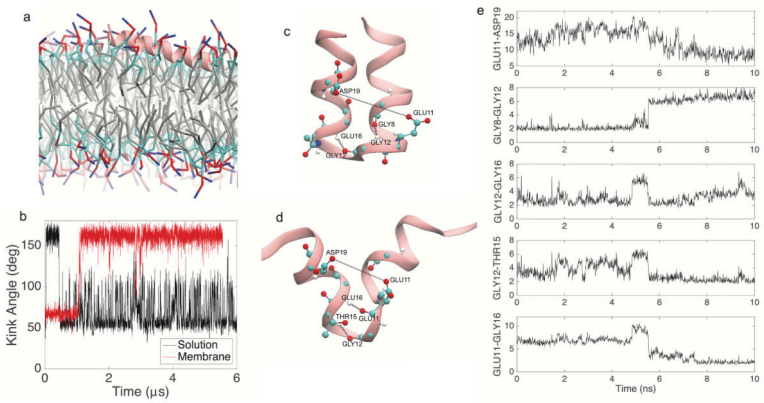

Figure 5.

HAFP Analysis. a) Centroid structure from simulation initiated in hairpin conformation on the membrane. b). Kink angles for simulations started from hairpin structure in solution and on membrane. c) NMR determined structure, the H-bonds involving GLY12 and the distance between ASP19 and GLU11 are shown. d) Structure at 10 ns, for simulation starting in hairpin on the membrane. Distances between ASP19 and GLU11 side chain oxygens as well as H-bonds involving GLU11 and GLY12 are shown. e) Distance of first 10ns of membrane bound simulations of the distance pairs denoted in subfigures (c) and (d).